SRNL Shelf Life Studies – SCC Studies at Room Temperature

J. I. Mickalonis

J. M. Duffey

November 2014

SRNL-STI-2014-00418, Revision 0

DISCLAIMER

Printed in the United States of America

Prepared for
U.S. Department of Energy

SRNL-STI-2014-00418
Revision 0

Keywords: *3013 plutonium storage, stress corrosion cracking, pitting*

Retention: *Permanent*

SRNL Shelf Life Studies – SCC Studies at Room Temperature

J. I. Mickalonis
J. M. Duffey

November 2014

Savannah River National Laboratory
Savannah River Nuclear Solutions, LLC
Aiken, SC 29808

Prepared for the U.S. Department of Energy under contract number DE-AC09-08SR22470.

ACKNOWLEDGEMENTS

The authors wish to acknowledge the following for their assistance in conducting the experimental work and metallurgical evaluations: H. M. Ajo, M. S. Blume, K. P. Crapse, M. L. Crowder, F. A. Foreman, M. Y. Hightower, M. A. Lee, W. B. Matthews, S. W. McCollum, B. Y. Mealer, D. A. Mitchell, T. R. Murphy, T. Reown, D. S. Scott, and V. B. Timmerman.

EXECUTIVE SUMMARY

Phase II, Series 2 corrosion testing performed by the Savannah River National Laboratory (SRNL) for the Department of Energy 3013 container has been completed. The corrosion tests are part of an integrated plan conducted jointly by Los Alamos National Laboratory and the Savannah River Site. SRNL was responsible for conducting corrosion studies in small-scale vessels to address the influence of salt composition, water loading, and type of oxide/salt contact on the relative humidity inside a 3013 container and on the resulting corrosion of Type 304L and 316L stainless steel (304L and 316L). This testing was conducted in two phases: Phase I evaluated a broad spectrum of salt compositions and initial water loadings on the salt mixtures exposed to 304L and 316L and the resulting corrosion; Phase II evaluated the corrosion of 304L at specific water loadings and a single salt composition.

During Phase I testing at high initial moisture levels (0.35 to 1.24 wt%)[a], the room-temperature corrosion of 304L exposed to a series of plutonium oxide/chloride salt mixtures ranged from superficial staining to pitting and stress corrosion cracking (SCC). 304L teardrop coupons that exhibited SCC were directly exposed to a mixture composed of 98 wt % PuO_2, 0.9 wt % NaCl, 0.9 wt % KCl, and 0.2 wt % $CaCl_2$. Cracking was not observed in a 316L teardrop coupon.

Pitting was also observed in this environment for both 304L and 316L with depths ranging from 20 to 100 µm. Neither pitting nor SCC was observed in mixtures with a greater chloride salt concentration (5 and 28 wt%). These results demonstrated that for a corrosive solution to form a balance existed between the water loading and the salt chloride concentration. This chloride solution results from the interaction of loaded water with the hydrating $CaCl_2$ salt.

In Phase II, Series 1 tests, the SCC results were shown to be reproducible with cracking occurring in as little as 85 days. The approximate 0.5 wt% moisture level was found to result in an initial relative humidity of ~55% within the small-scale vessels. Pits were found to be associated with cracks and appeared to act as initiators for the cracking. In a vapor-space only exposure, the weld oxide, which results from the TIG closure weld used to fabricate the teardrop coupon, was also shown to be more susceptible to pitting corrosion than a surface free from weld oxide. This result has important implications for the closure weld of the 3013 inner can since the weld oxide on the can internal surface cannot be removed.

The results from the Phase II, Series 2 tests further demonstrated the significance of forming a solution with a critical chloride concentration for corrosion to proceed. 304L teardrop coupons were found to corrode only by pitting with a similar oxide/salt mixture as used in Series 1 testing but with a lower water loading of 0.2 wt%, which resulted in an initial relative humidity of 35-38%. These tests ran twice as long as those for Series 1 testing. The exposure condition was also found to impact the corrosion with salt-exposed

[a] The 3013 limit on water content is 0.5 wt%.

surfaces showing lower corrosion resistance. Additional analyses of the Series 2 coupons are recommended especially for determining if cracks emanate from the bottom of pits.

Data generated under the 2009 3013 corrosion test plan, as was presented here, increased the understanding of the corrosion process within a sealed 3013 container. Along with the corrosion data from destructive evaluations of 3013 containers, the inner can closure weld region (ICCWR) has been identified as the most vulnerable area of the inner can where corrosion may lead to corrosive species leaking to the interior surface of the outer container, thereby jeopardizing the integrity of the 3013 container. A new corrosion plan has been designed that will characterize the corrosion at the ICCWR of 3013 DEs as well as parameters affecting this corrosion.

TABLE OF CONTENTS

LIST OF TABLES

LIST OF FIGURES

LIST OF ABBREVIATIONS

DE	Destructive Examination
DOE	Department of Energy
EDS	Energy Dispersive Spectrocopy
ICCWR	Inner Can Closure Weld Region
LANL	Los Alamos National Laboratory
M&TE	measuring and testing equipment
RH	relative humidity
SCC	stress corrosion cracking
SEM	scanning electron microscope
SRNL	Savannah River National Laboratory
TD	teardrop
TIG	tungsten inert gas
304L	Type 304L stainless steel
316L	Type 316L stainless steel

1.0 Introduction

An integrated test plan by Savannah River (SRNL) and Los Alamos (LANL) National Laboratories was initiated in 2009 to focus studies on the susceptibility of 3013 storage containers to stress corrosion cracking (SCC) [1]. These corrosion studies were designed to validate the assumptions in the Department of Energy (DOE) Standard DOE-STD-3013 as well as provide essential information to augment field surveillance data collected at 3013 storage sites [2]. Important variables included the influence of temperature, salt composition, moisture, residual stress and exposure (salt contact or vapor space over the salt) on the relative humidity (RH) inside a 3013 container and the initiation and propagation of SCC. At SRNL, the studies evaluated the impact of moisture and exposure conditions on SCC initiation including its occurrence in conjunction with corrosion pits. The last series of tests were conducted at low water loading (0.2 wt%) to evaluate water loading conditions that had been reported during packaging and to determine if relative humidity conditions closer to the salt deliquescence point were more aggressive as suggested by the literature [5, 6]. These tests were completed in FY14 and the results are presented herein.

2.0 Purpose of Testing

Corrosion studies are part of the long-term surveillance program required by the Department of Energy (DOE) Standard DOE-STD-3013 and designed to validate the assumptions within the standard. Another integral part of the surveillance programs is field surveillance of 3013 containers at storage sites [1]. A mode of failure for the 3013 container identified by the standard for austenitic stainless steels is chloride SCC. The specified materials of construction for the 3013 inner and outer containers are Types 304L (304L) and 316L (316L) stainless steel, which are grades of austenitic stainless steel.

For SCC to occur, three parameters are needed to be present: a susceptible material, a stress (applied or residual), and a conducive environment. Much literature is available that demonstrates the susceptibility of austenitic stainless steels to chloride SCC [15]. Previous testing has demonstrated that there are sufficient stresses to cause cracking in both the 3013 inner and outer containers [16]. The corrosion studies have been focused on evaluating the third parameter of a conducive environment to cause cracking within a 3013 container. That environment will contain some level of moisture (loading-environment humidity) and concentration of plutonium oxide (radiation) and salt (chloride) at an elevated temperature (radioactive decay heat). Within the 3013 container, the cracking process requires the formation of a salt solution, resulting from deliquescence of contained salts, on the container surface in an area with sufficient stress, such as near welds or changes in container diameter.

The SRNL studies were performed in two phases: Phase I evaluated a broad spectrum of salt compositions and initial salt moistures for both 304L and 316L; and Phase II evaluated the corrosion of 304L at specific water loadings and a single salt composition. Results from the Phase I testing demonstrated that at bounding moisture conditions (0.6 wt% water loading) SCC occurred in 304L teardrop coupons at room temperature

exposed to a plutonium oxide/chloride salt mixture containing $CaCl_2$ [3]. A 316L teardrop coupon did not crack when exposed to identical conditions, although more time may have been required to initiate and grow a crack. Furthermore, the Phase I testing showed that cracking does not occur if the available moisture is insufficient to deliquesce salts and that the salt with the lowest deliquescent relative humidity will most likely be involved in the cracking process. The results from Phase I testing are summarized in Table 2-1

Phase II testing, which consisted of two series of tests, was targeted at measuring relative humidity inside the test containers during exposure and evaluating susceptibility to SCC at more realistic water loading conditions near the 3013 limit (<0.5 wt%). The first series, which was similar to Phase I testing except with the inclusion of a relative humidity probe, established that at the bounding water content within the 3013 standard realistic compositions existed which lead to SCC when susceptible material was exposed directly to the salt [4]. The observed cracking was found to be associated with pits that also formed during exposure. Pitting, although not cracking, was also found to be prevalent at the closure weld for the teardrop coupon. The results from Phase II testing are summarized in Table 2-1

The lower pitting resistance of this area of the teardrop coupon results from the presence of the weld oxide that formed during the welding and was not removed. During the formation of the weld oxide a chromium depletion layer within the material forms just below the oxide thereby increasing corrosion susceptibility.

Table 2-1 Summary of SRNL Corrosion Test Results for 3013 Storage Containers

Test	Chloride Salt (wt%)*	Moisture (wt%)	Maximum Test Time (days)	Corrosion Observation
Phase I	None	0.38	325	Staining
	28%	0.94-1.0	489	Staining
	2% ($MgCl_2$)	0.35	274	Staining
	2% (0.2% $CaCl_2$	0.5-0.68	506	SCC
	2% (0.9% $CaCl_2$	0.61-0.66	496	Pitting
	5% ($MgCl_2$)	0.45-1.24	470	Pitting
Phase II, Series 1	2% (0.2% $CaCl_2$	0.45-0.59	340	SCC
Phase II, Series 2	2% (0.2% $CaCl_2$	0.16-0.18	774	Pitting

* Chloride salts are composed principally of NaCl and KCl.

3.0 Test Configuration

The preparation of the test vessel and components for Phase II tests were identical to that used during Phase I testing [3] with the exception of a humidity sensor incorporated into the vessel lid. The details of those preparation steps and the loading of the test vessels are presented in this section.

3.1 PuO_2/Salt Preparation

The PuO_2 and chloride salt mixture used throughout Phase II had a target composition of 98 wt% PuO_2, 0.85 wt% NaCl, 0.85 wt% KCl, and 0.3 wt% $CaCl_2$. This composition was selected to replicate that used when SCC was observed previously in Phase I test of the small-scale corrosion tests [3]. The chloride salts used in this testing were taken from a master batch of a chloride salt mixture previously prepared for non-rad humidity tests [7]. The PuO_2 was taken from material known as PEOF1, which was received from LANL. PEOF1 is a high purity (87.8% Pu) oxide prepared by nitric acid anion exchange oxalate precipitation and calcination to 600 °C to produce PuO_2 followed by additional calcination to 975 °C for four hours [8].

For the preparation of the chloride salt mixture, most steps were performed in an argon-inert glovebox, where humidity levels were generally below 500 ppm. The requisite quantity of each chloride salt was weighed for a total mixture quantity of 500 g. The balance and calibrated weight set were compliant with M&TE controls. The salts were mixed together and heated to 825 °C for fifteen minutes after which the salts were visually confirmed to have melted. Pre- and post-heating weight measurements of the salt mixture showed a difference of approximately 0.15%, indicating minimal losses during heating. The fused salts were ground with a mortar and pestle and stored in a glass vial in the inert glovebox until needed.

Prior to mixing the PuO_2 with the salt mixture, the oxide was dried in a furnace housed in an air glovebox. The oxide was heated to over 300 °C for approximately 15 minutes then cooled to less than 150 °C prior to mixing with the salt mixture. The salt mixture was pre-weighed in the argon glovebox where it was stored and packaged in double containment (screw-lid glass jar placed in a plastic jar with 4Å molecular sieve) for transfer to the air glovebox. The oxide/salt mixture was prepared by combining 52.05 g of PuO_2 with 1.1 g of the chloride salt mixture. The oxide/salt mixture was placed in a covered crucible and heated to 825 °C and held for 15 minutes. The oxide/salt mixture was cooled to less than 150 °C and then packaged for transfer in a double containment similar to that used for the salt mixture.

3.2 Test Coupons

The test coupons were fabricated from 304L and were teardrop shaped. The coupons were from the same initial set purchased at the start of Phase I testing and were as-fabricated from Metal Samples Inc. (Munford AL). The teardrop coupons are used as a screening tool to assess susceptibility to SCC as well as pitting corrosion. A teardrop coupon, as shown in Figure 3-1 (A), is fabricated by bending a rectangular strip (0.75 in × 4 in × 0.065 in) around a 1-inch mandrel and joining the ends by tungsten inert gas (TIG) welding. The teardrop coupons had a transverse autogenous weld at the center of curvature in the rounded section to provide a similar weld microstructure as is present in the inner 3013 container closure weld region (ICCWR).

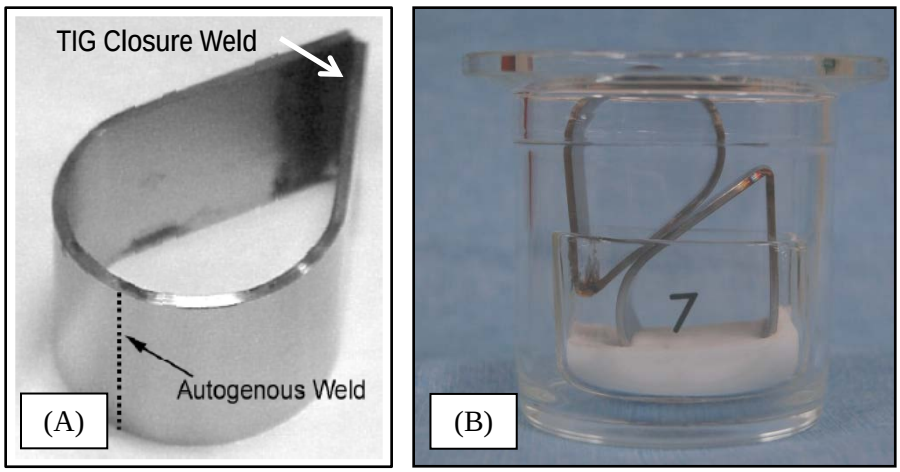

Figure 3-1 (A) Teardrop coupon for SCC testing with the autogenous weld centerline indicated by the dotted line and a TIG closure weld and (B) Arrangement of oxide/salt-contact and vapor-exposed teardrop coupons in test vessel (actual test vessel is made of stainless steel)

3.3 Test Vessels

The test vessels as shown in Figure 3-2 were fabricated from 304L. A design flange with a welded bottom, approximately 2 in. diameter and 2.5 in. tall, was used for the bottom section. The vessel lid flange had Swagelok fittings welded in place for a thermocouple, pressure sensor, humidity probe, and a valve for gas sampling. The pressure sensors were purchased from General Electric (Billerica, MA) and were modified by welding to a 0.125-in. adapter. The humidity probes and thermocouples were supplied by EdgeTech (Marlborough, MA) and Omega (Stamford, CN), respectively.

Figure 3-2 Test vessel with pressure sensor, humidity probe, thermocouple, and gas sampling capability

The dish to hold the oxide/salt mixture was made of borosilicate glass as shown in Figure 3-1 (B). The vessel components were helium leak tested for leak tightness [9]. The vessel bodies without the humidity probe passed the leak test and showed a rate of helium leakage of 10^{-9} std cc/s at a pressure of 1 atm. However, placement of the humidity probes generally increased the leakage and caused the leak rates to vary between 10^{-3} to 10^{-9} std cc/s. Several attempts were made to seal the probes with epoxy, but these attempts were of limited success.

3.4 Pressure Gage, Humidity Probe, and Thermocouple Calibrations

Each pressure gage, humidity probe and thermocouple was calibrated prior to the start of testing.

3.4.1 *Pressure Gage*

The GE NovaSensor NPI-19 pressure sensors were calibrated by comparing the sensor response against a calibrated M&TE pressure transducer. The calibration was accomplished by connecting 11 test sensors and the M&TE sensor to a common manifold. The manifold was evacuated until at a stable pressure of 0.01 kPa (0.075 Torr) as measured by the M&TE sensor. The voltage output of each pressure sensor was recorded. The manifold pressure was increased in increments of approximately 65 to 130 kPa (488 to 975 Torr) to a maximum pressure of 670 kPa (5025 Torr) while recording the voltage output of each step change for all the test sensors. This step was repeated while decreasing the pressure back to 0.01 kPa. Calibrations were performed at 22, 23, and 25 °C because the sensor response varies with temperature. These data were used to construct calibration curves for each sensor.

3.4.2 *Humidity Probe*

The humidity probes were calibrated using a programmable chilled mirror chamber supplied by EdgeTech (Marlborough, MA) with a RH accuracy of 0.5% over the range of 5-95% (RH CAL portable humidity calibrator). Several probes were inserted into the chamber simultaneously and tested over a RH range of 5-75% at a temperature of 25 °C. Probes were allowed to stabilize at each humidity level for at least 1.5 hours (usually between 2 and 3 hours).

3.4.3 *Thermocouple*

The thermocouples were checked using a Hart Scientific, Model 9107, dry-well calibrator (M&TE) over the temperature range of 10-90 °C. The thermocouples were allowed to equilibrate to a set point for approximately two hours. When the set point was either 20 or 30 °C, the thermocouple values varied from the set point by 0.3 to 0.6 °C and at temperatures above 50 °C, the variation from the set point was up to 2 °C.

3.5 Loading Test Vessels

A helium-purged glovebag deployed inside a radiological glovebox was used to prepare the test vessels in a humidity-controlled helium atmosphere. Water was loaded to the oxide/salt mixtures and packaged with the teardrop coupons into instrumented test vessels. Glovebag RH was controlled by independently adjusting the flow rates of dry and humidified helium streams. Dry helium from a bank of helium cylinders was split

into two streams that had independent mass flow controllers. One of the split streams of helium passed over a humidifying membrane, while the other stream was unaltered. The two streams were recombined into a single stream before entering the glovebox and glovebag. The total flow rate was maintained relatively constant at about 10 standard liters per minute. The humidity of the recombined stream was determined by passing a side stream over a chilled mirror dew point hygrometer. A separate humidity probe inside the glovebag was used to monitor changes in the bag humidity. The glovebag was at ambient glovebox temperature.

The glovebag was first purged with dry helium for two hours at a flow rate of 10.0–10.5 standard liters per minute. During this time the glovebag RH decreased from approximately 15% to a minimum of approximately 6% at a temperature of 23 ± 0.2 °C. The analytical balance calibration was verified using a set of calibrated weights ranging from 1 to 200 g. The jar containing the oxide/salt mixture (in air atmosphere) was then opened, closed, and weighed repeatedly until a constant weight was obtained, indicating the air was displaced with helium. Next, nominally 5 g of the oxide/salt mixture was weighed into a glass "boat" insert as shown in Figure 3-1 (B).

One teardrop coupon was placed in the boat on top of the oxide/salt mixture, and a second portion of mixture (nominally 10 g) was added to the boat within the closed loop of the teardrop coupon. The glass boat insert was placed into a small stainless steel pan for ease of handling. This process was repeated for each of three replicate coupons.

The RH in the glovebag was gradually increased for loading moisture on to the oxide/salt mixture. The small stainless steel pans holding the sample sets were weighed periodically in the humidified helium atmosphere until the weight gain of each sample set corresponded to a water uptake of about 0.16 wt%. The amount of water loading was targeted with the goal of obtaining a RH in the sealed test container of approximately 22%. The purge stream RH, glovebag RH, and mass gain of each Series 2 sample set are shown in Figure 3-3 as a function of time.

As each sample set reached the targeted water loading, the glass insert containing the oxide/salt mixture and teardrop coupon was placed into a stainless steel test vessel. The second teardrop coupon was then placed on top of the first coupon as shown in Figure 3-1 (B), and the vessel was sealed by compressing a metal gasket between upper and lower flanges held together by a chain clamp encircling and overlapping the outer edges of the two flanges. This process was repeated for each of the three sample sets. The initial fill gas of each vessel was nominally 100 kPa of helium.

The sealed test vessels were removed from the helium glovebag, bagged out of the glovebox, and transferred to a separate air-atmosphere radiological glovebox for the test duration. The test vessels were connected to the computer data acquisition module within 24 hours of being sealed. The computer data acquisition system electronically monitored and recorded internal pressure, temperature, and relative humidity for each test vessel.

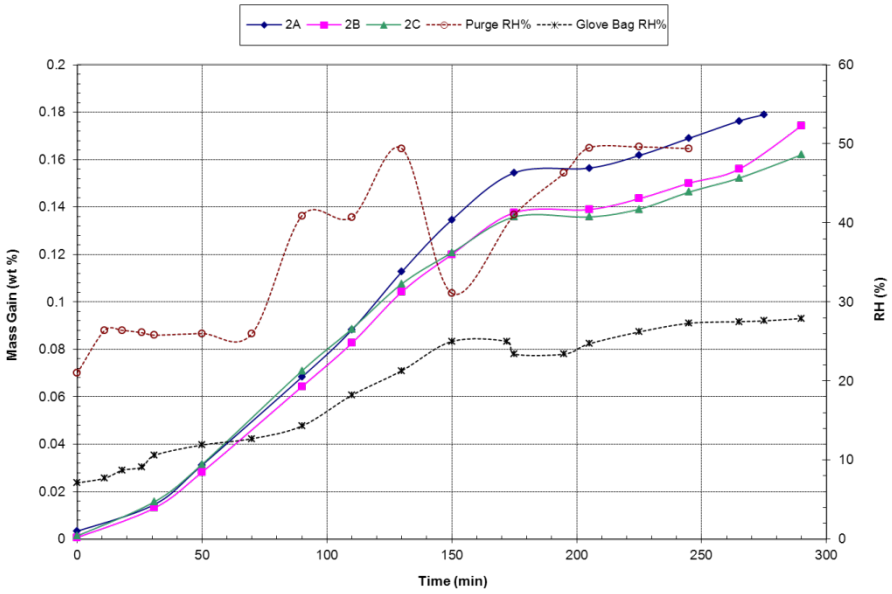

Figure 3-3 Sample mass gain, purge RH, and glovebag RH as a function of time during exposure of teardrop coupons and oxide/salt mixtures to humidified helium atmosphere for loading Series 2 test vessels

3.6 Post Test Analysis

At the conclusion of a test, a gas sample of the head space for each vessel was pulled for analysis by gas chromatography. Work was performed quickly since the glovebox was not humidity controlled. The teardrop coupons were digitally photographed to document the as-is condition. The coupons were cleaned in 0.1 M nitric acid solution to remove corrosion products. A small brush was used to dislodge any adherent corrosion product. This cleaning step was not sufficient to remove adherent oxides, especially within pits. Coupons were dried and then photographed again. Coupons were examined in the scanning electron microscope (SEM) to determine if small cracks were observed on the surface. Within the SEM, coupon surface chemistry was evaluated using Energy Dispersive Spectroscopy (EDS). Coupons from Vessel were also examined using a stereomicroscope.

4.0 Humidity and Pressure Trends during Exposure

The RH, temperature, and pressure trends of the three test vessels are shown in Figure 4-1. Data acquisition failed for a short period after approximately 300 days, but performed reliably for the remainder of the test. Although the target RH was approximately 22% the initial RH of all three test containers was in the range of 35-40%. The higher RH indicated that more water was present in the test cell than planned [4]. The pressure probe in Vessel B generated an intermittent signal after approximately 75 days into the test. Troubleshooting was unsuccessful. The temperature of the test vessels varied from approximately 16 to 24 °C, varying with the ambient room temperature.

The vessels were opened in the order of A, B, and C after 131, 405, and 774 days, respectively. The relative humidity of Vessel A was fairly constant over the entire

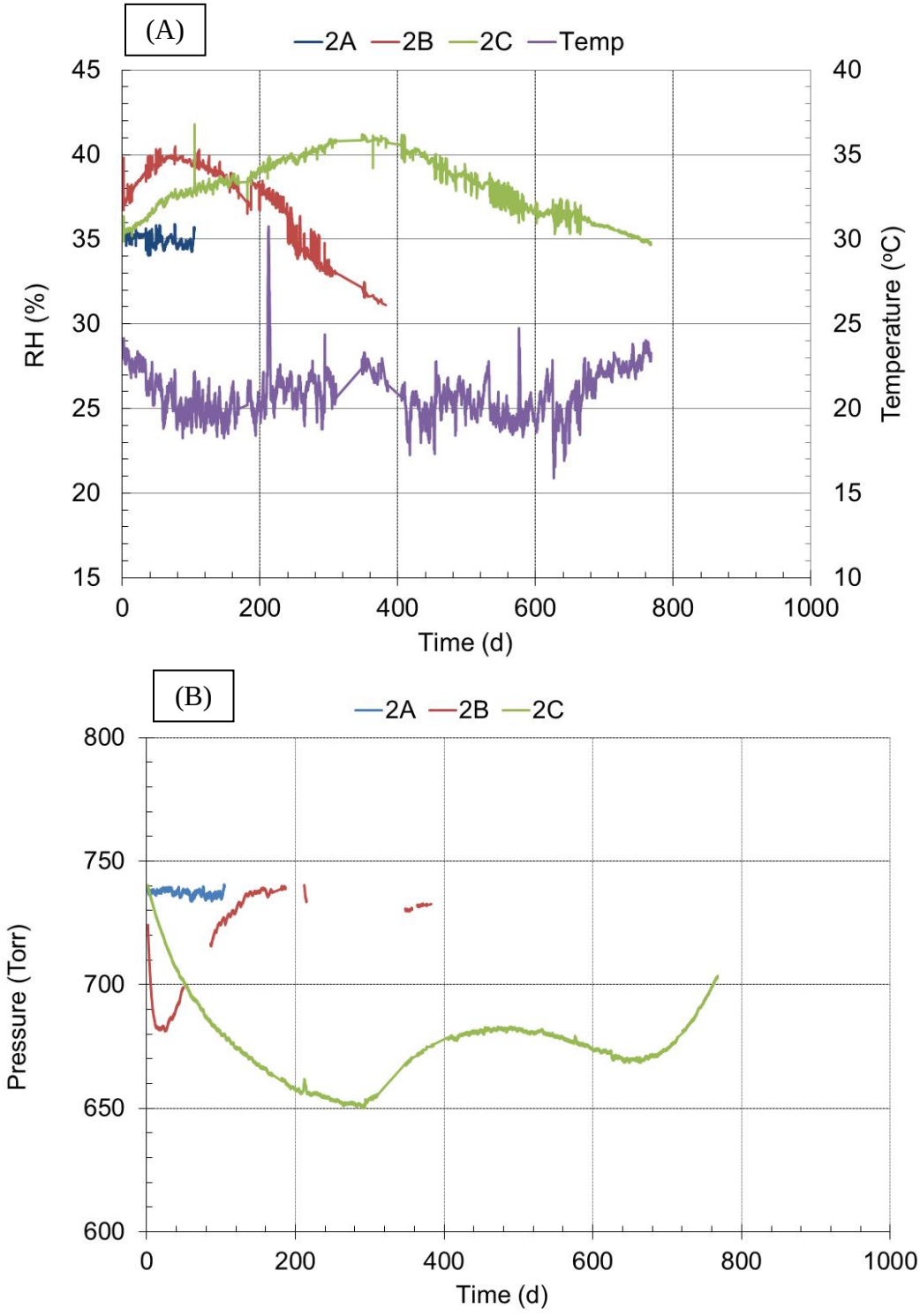

Figure 4-1 Trends in exposure conditions for Series 2 test: (A) relative humidity and temperature and (B) pressure

exposure period at 35% as was the pressure trend at 740 Torr. Both Vessels B and C showed an increase in the humidity followed by a corresponding decrease, although the periodicity differed for the two vessels. Vessel B varied in a humidity range of 31 to 40%, while Vessel C had a humidity range of 34 to 41%. The pressure trends for Vessels B and C were the inverse of their humidity trend, decreasing then increasing after some time period.

Prior to opening each test vessel, a gas sample from the head space was taken by expanding into a pre-evacuated 150-ml sample vial for analysis by gas chromatography. The results are shown in Table 4-1. Vessel A was thought to have been opened to the atmosphere since the measured pressure, 740 Torr, is close to atmospheric pressure. The gas analysis, however clearly showed that the initial helium atmosphere from the glovebox was still present after 131 days.

Table 4-1 Headspace Gas Composition (vol %) for Series 2 Test Vessels*

Vessel	He	H_2	O_2	N_2	N_2O
A	97	1.6	<0.1	0.34	<0.1
B	0.76	0.2	15	80	0.7
C	22	0.1	7.0	68	0.8

* CH_4, CO_2, and CO were not detected

Vessel B was also considered to have leaked due to reaching atmospheric pressure before opening after going through a pressure decrease. The gas composition was found to be similar to air. Finally, Vessel C had increasing pressure near the end of the test approaching atmospheric pressure. The gas still had significant helium but also the presence of oxygen and nitrogen. For Vessels B and C, the pressure rise indicated a leak to the atmosphere.

5.0 Corrosion of 304L Teardrops

At the level of moisture added for Series 2, SCC was not observed in any teardrop coupon over the 774 days of the test. Pitting was present on all coupons, although results differed for the two exposure conditions (oxide/salt and vapor only) of each coupon. Table 5-1 presents a summary of the exposure conditions and corrosion for the teardrop (TD) coupons along with exposure conditions.

Table 5-1 Teardrop Coupons Exposure Conditions and Corrosion Status

Vessel	TD #	Exposure Condition	Added Water (wt %)	Pressure	Exposure Time (days)	Corrosion
A	16	Oxide/Salt	0.18	Constant	131	Pitting
	18	Vapor				Pitting
B	15	Oxide/Salt	0.17	Dropped then increased	405	Pitting
	19	Vapor				Pitting
C	17	Oxide/Salt	0.16	Dropped then increased	774	Pitting
	20	Vapor				Pitting

The three test vessels, A, B, and C, were removed at times of 131, 405, and 774 days, respectively. The times were approximately double those for the Series 1 test vessels since corrosion was expected to be less severe due to the lower water concentration. A particular vessel was chosen to be opened at the designated time based on the pressure trend.

5.1 Vessel A – 131-day Exposure

Vessel A had both a constant humidity level and pressure over the test period, while the gas composition was principally helium. The teardrop coupon in contact with the oxide/salt mixture (TD16) experienced more corrosion than the coupon exposed only in the vapor space (TD18) as shown in Figure 5-1 (A), (B) and (C) for the as-is condition. Pitting was observed on the interior surface of TD16 as shown in Figure 5-1 (B). From the pitting observed on TD16, the coupon may have shifted such that the autogenous weld (not the closure weld) on the apex of the coupon was nearly out of the oxide/salt oxide/salt mixture. The test vessels are bagged out of the glovebox used for loading the cells and transported to another glovebox for the test duration so adjustment in initial position is not unexpected.

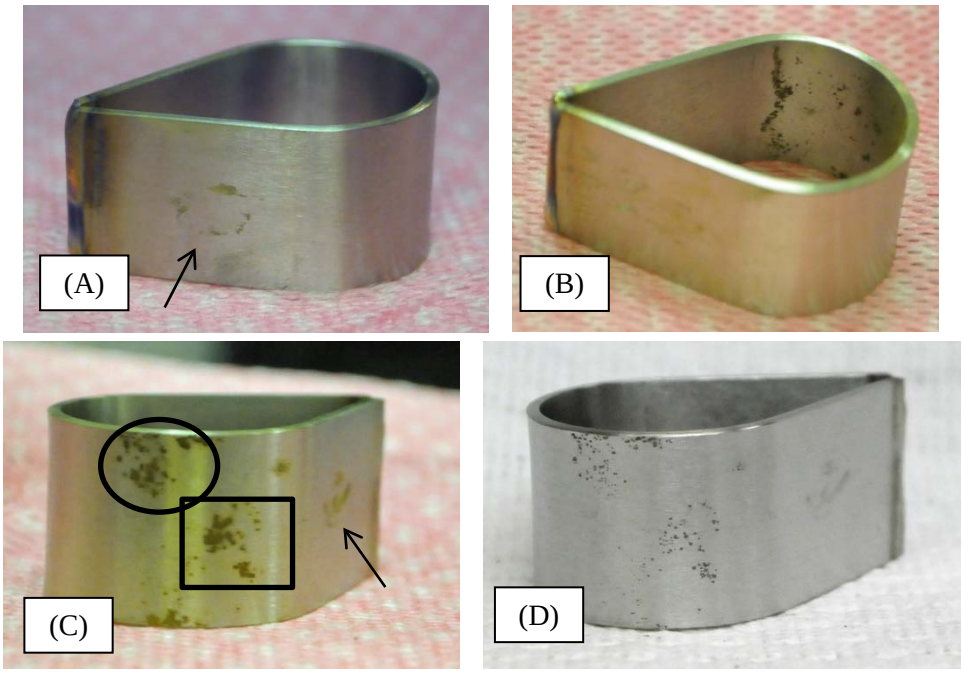

Figure 5-1 Photographs of Vessel A teardrop coupons after 131-day exposure: (A) TD18, vapor exposure, as-is condition; (B and C) TD16, oxide/salt contact, as-is condition; and (D) TD16, oxide/salt contact, after nitric acid cleaning

Both coupons had an apparent corrosion spot on the flat region of the teardrop on the exterior surface (shown by the black arrow in the Figure 5-1 (A) and (C)). This area was not examined closely on these coupons but was examined in greater detail on teardrop coupons with longer exposure time, where there is further discussion. Minimal corrosion

was observed on the TIG closure weld as can be seen in Figure 5-1 (A) and (B) for the vapor and oxide/salt exposure, respectively.

The exterior surface of TD16, the teardrop coupon in the oxide/salt mixture, was observed on the SEM. TD 18 was not examined due to the minimal corrosion observed. The marked regions in Figure 5-1 (C) show where on the coupon the pitting was examined. Pitting similar to that observed during the Phase II, Series 1 testing was found. Figure 5-2 shows the pits on TD16 from both the marked region in Figure 5-1 (C). Pits were variable in size (ten to hundreds of microns) and appeared to be shallow. Smaller pits tended to be circular while the larger pits tended to be elongated. No further pit characterization was performed.

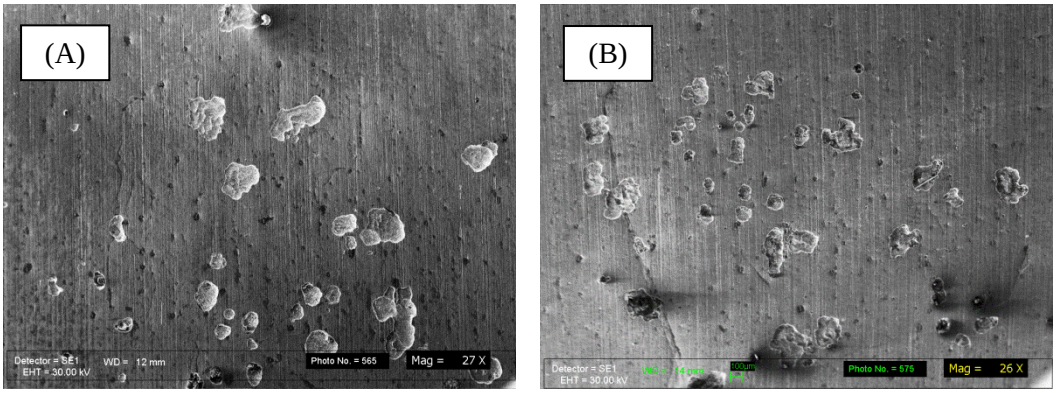

Figure 5-2 SEM micrographs of pitting on coupon TD16: (A) pitting in area near autogenous weld, shown as the circled region in Figure 4-1 (C) (27x); and (B) pitting in an area away from autogenous weld, shown as the squared region in Figure 4-1 (C) (27x)

5.2 Vessel B – 405-day Exposure

Vessel B pressure and humidity had an inverse trend with an initial pressure drop and humidity rise followed by a pressure increase and humidity drop. The vessel was found to have leaked with oxygen and nitrogen as found in the post-test gas analysis. The teardrop coupon (TD15) in contact with the oxide/salt mixture experienced more corrosion than the coupon exposed only in the vapor space (TD19) as shown in Figure 5-3 (A) and (B) for the as-is condition. The TIG closure weld on both coupons had more significant corrosion products than the coupons from Vessel A. Numerous pits can be seen on TD15 on both the interior and exterior surfaces.

Coupons TD15 and TD19 were examined more closely with both a stereomicroscope and SEM. For both coupons, pitting occurred in the weld oxide of the TIG closure weld with the pitting greater on the TIG closure weld of TD19, the vapor-exposed coupon. Figure 5-4 shows the difference in pitting between these two coupons. This greater pitting is attributed to the orientation of the vapor-exposed coupon where the TIG closure weld is closer to the oxide/salt mixture.

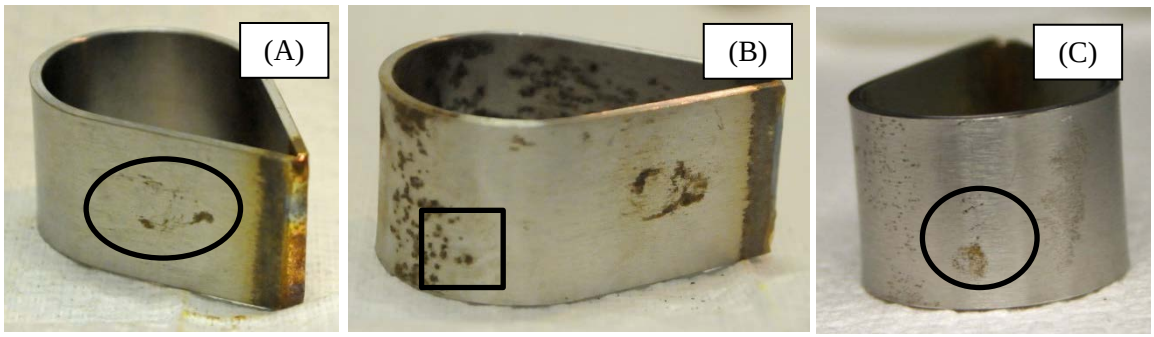

Figure 5-3 Photographs of Vessel B teardrop coupons after 405-day exposure: (A) TD19, vapor exposure, as-is condition (circled area shows corrosion); (B) TD15, oxide/salt contact, as-is condition; and (C) TD15 after nitric acid cleaning

As can be seen in Figure 5-4 (B), the vapor-exposed coupon (TD19) has pits occluded with oxide or corrosion products as well as opened pits. Sufficient moisture and chloride migrated to the surface for the corrosion to progress. Any chlorides may have resulted from either vapor transport or salt displacement. In Phase II, Series 1 tests, this difference between the vapor-exposed coupon and salt-exposed coupon were similar, although the disparity in pit densities was not quite as marked [4].

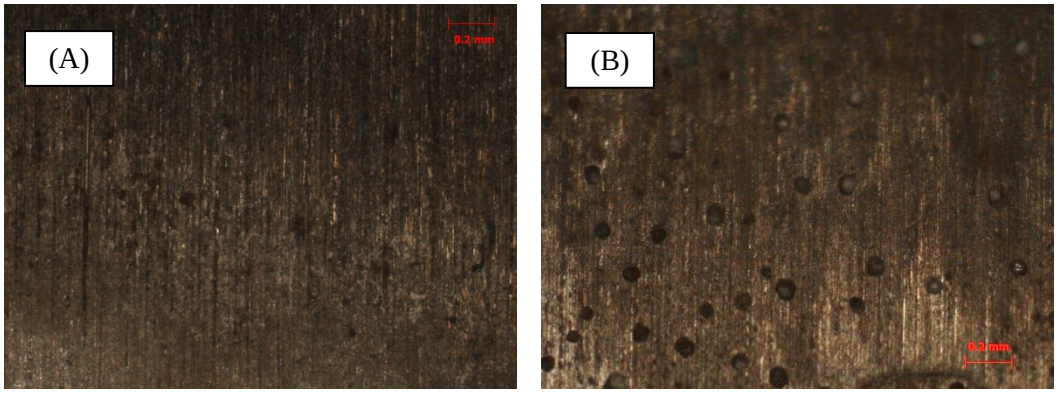

Figure 5-4 Photographs of pitting in the TIG closure weld region of teardrop coupons TD15 (A) and TD19 (B) as viewed through a stereomicroscope (63x)

The findings on the TIG closure weld of these teardrop coupons is important because they apply directly to the TIG closure weld for the 3013 inner can. The difference between the two is that stresses sufficient for SCC are known to exist for the inner can closure weld region [10]. The results for the teardrop coupons show that these areas are more susceptible to corrosion. This corrosion occurs even in the absence of high stress and is attributed to the formation of the surface oxide, a chromium depletion layer beneath the oxide and other changes to the microsturcture and micro-chemistry of the metal that are a result of welding. The effect of the oxide can be clearly seen in Figure 5-5 where the pitting is observed in the oxide covered areas only.

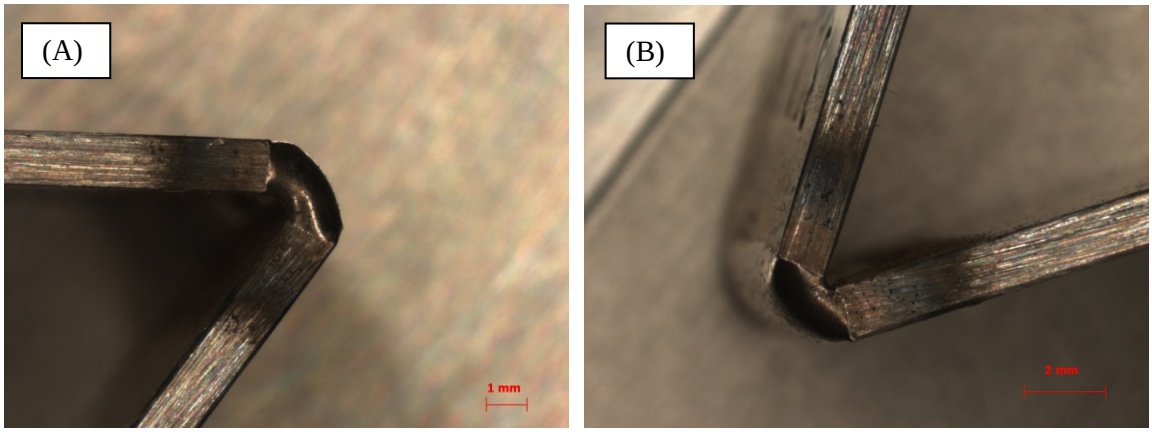

Figure 5-5 Photographs of pitting along the edges of teardrop coupons TD15 (A) and TD19 (B) as viewed through a stereomicroscope (10x)

Another feature observed previously in teardrop coupons from the Phase II, Series 1 tests is the array of small pits that at low magnification appear like cracks [4]. These arrays were observed on both coupons as shown by the photographs in Figure 5-6. The mechanism for the formation of these pit arrays has not been determined. Another noteworthy feature is the rust-colored corrosion products seen in Figure 5-6 (B), which suggests sufficient oxygen was available in the system. For Vessel B, the measured oxygen concentration was 15 vol%, which equals a partial pressure of 110 Torr.

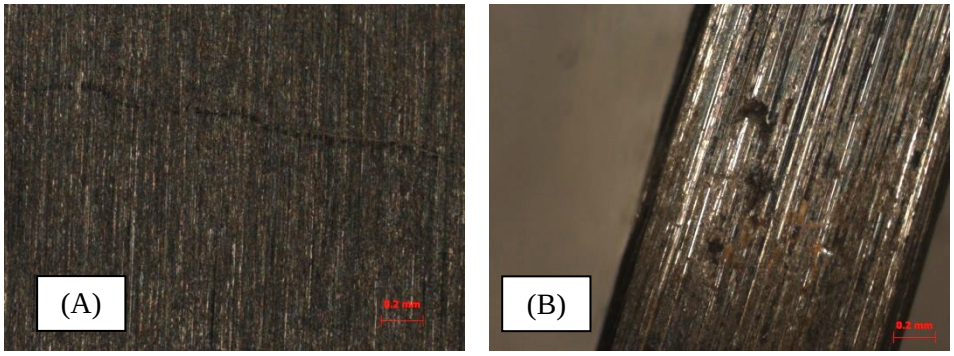

Figure 5-6 Photographs of teardrop coupons show the pit arrays which form in the vapor space as viewed through a stereomicroscope: (A) TD15 (63x); and (B) TD19 (63x)

Similar to observations on previous teardrop coupons exposed to the oxide/salt mixture, the population of pits showed both large and small diameter pits. This bimodal population was observed both at the autogenous weld and away from it as shown by the SEM micrograph in Figure 5-7. The pit population was greater at the autogenous weld than away from it, which differed from Vessel A coupons where the pit populations appeared more equivalent.

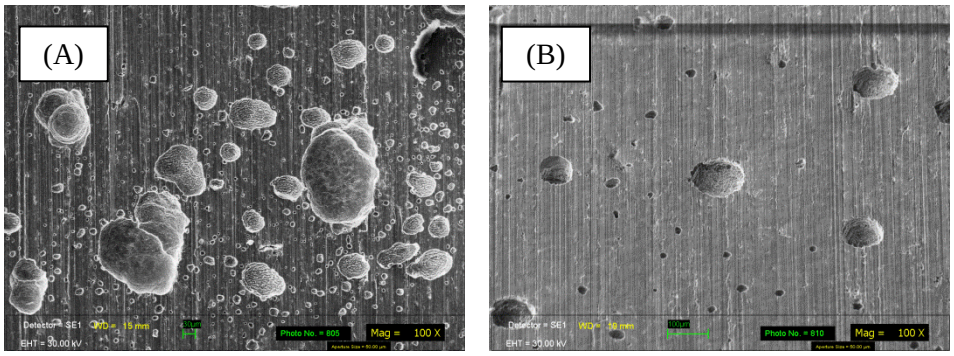

Figure 5-7 SEM micrographs of pitting on coupon TD15: (A) pitting in area near autogenous weld, shown as the circled region in Figure 5-3 (C) (27x); and (B) pitting in an area away from autogneous weld, shown as the squared region in Figure 5-3 (B) (27x)

The region of attack in the middle of the teardrop faces (circled in Figure 5-3 (A) and indicated by arrows in Figure 5-1 (A) and (C)) was examined more closely on the stereomicroscope and SEM where this attack was found to be pits. Similar markings were found on coupons from Phase II, Series 1 [4]. The pitting can be seen in Figure 5-8 for TD19, the vapor-exposed coupon. As can be seen some pits still have corrosion products inside (indicated by arrows in Figure 5-8 (A)). The pit morphology and bimodal population appear similar to those on TD15. This pitting is believed to be associated with the work hardening of the surface that occurs at these local spots during the bending of the coupon around the mandrel.

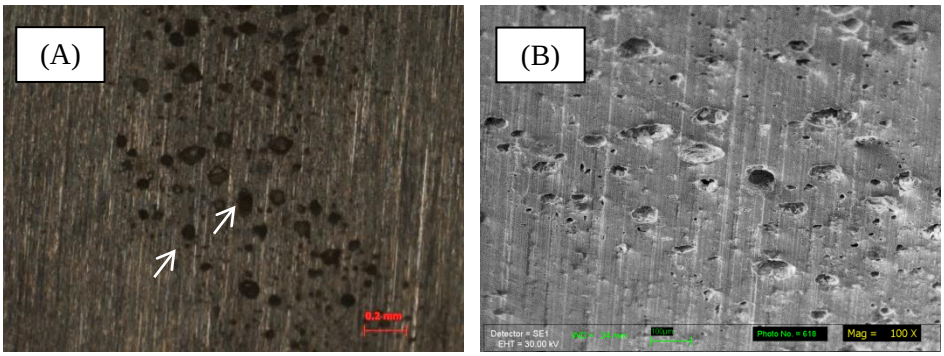

Figure 5-8 Stereomicroscope image (A) and SEM micrograph (B) of pitting on vapor-exposed coupon TD19 (see circled area in Figure 5-3 (A)): (A) 63x and (B) 100x

5.3 Vessel C – 774-day Exposure

Vessel C pressure and humidity had an inverse trend with an initial pressure drop and humidity rise followed by a pressure increase and humidity drop. The vessel was found to have leaked with oxygen and nitrogen found in the post-test gas analysis. The observations on these coupons are very limited due to budget restrictions when this last test vessel was opened. The observations were limited to photographing the coupons both before and after cleaning and a limited SEM investigation.

The teardrop coupon (TD17) in contact with the oxide/salt mixture experienced more corrosion than the coupon exposed only in the vapor space (TD20) as shown in Figure 5-9 for the as-is condition and after nitric acid cleaning. The TIG closure weld on both coupons had more significant corrosion products than the coupons from Vessels A and B.

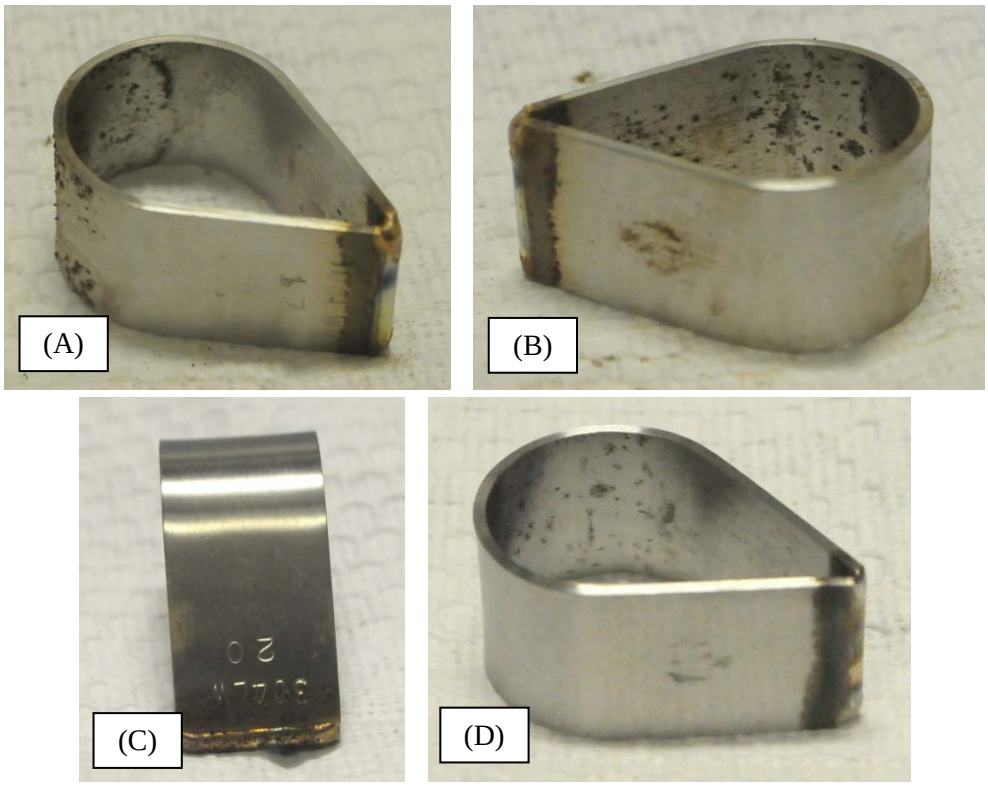

Figure 5-9 Photographs of Vessel C teardrop coupons after 774-day exposure: (A and B) D17, oxide/salt contact, as-is condition; (C) TD20, vapor exposure, as-is condition; and (D) TD17 after nitric acid cleaning

Numerous pits can be seen on TD17 on both the interior and exterior surfaces. Cracks were not observed on this coupon similar to other salt-exposed teardrop coupons in Phase II, Series 2 testing. The lack of cracking was confirmed by SEM observations as shown by the micrograph in Figure 5-10 (A). The bimodal population of pits (i.e. large and small) observed on other salt-exposed coupons can be seen here. This bimodal population was seen both within and outside the weld region.

A “pearl necklace” pit corrosion morphology was observed near the TIG closure weld for the coupon exposed only in the vapor space. Figure 5-10 (B) shows this morphology on TD20. This type of connected pits was also noted during Phase II, Series 1 testing. The mechanism for this type of pit formation or propagation is not known.

The TIG closure weld on both coupons had a buildup of corrosion products. Similar to other teardrop coupons in both test series the corrosion was greater on the vapor-exposed coupon, which was facing downward, than on the salt-exposed coupon. These results are clearly shown by the photographs in Figure 5-11.

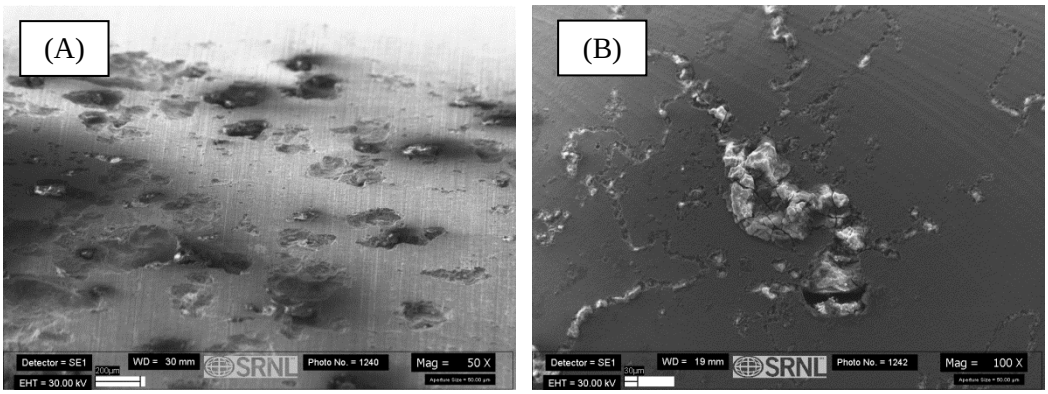

Figure 5-10 SEM micrographs of teardrop coupons from Vessel C after 774-day exposure: (A) TD17, pitting only in region of salt exposure (50x); and (B) TD20, 'pearl necklace' morphology of linked pits near TIG closure weld (100x)

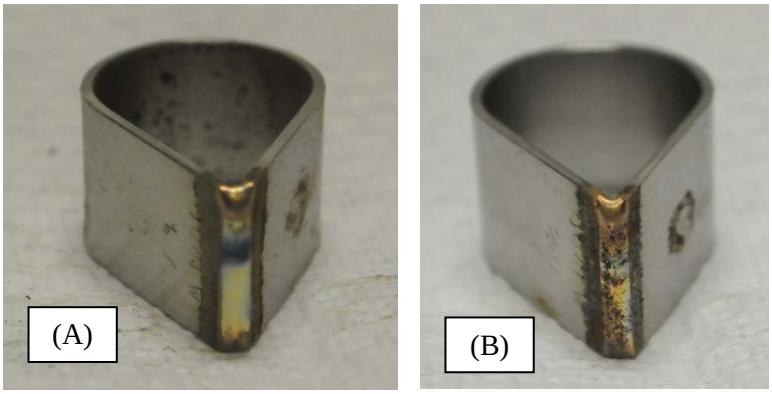

Figure 5-11 Photographs of TIG closure weld for teardrop coupons from Vessel C after 774-day exposure: (A) TD17, salt exposed and (B) TD20, vapor exposed

The presence of chloride on both samples was investigated in the SEM for areas near the TIG closure weld. The samples had been briefly cleaned in a 0.1M nitric acid solution, but the chloride that would be incorporated into the oxide or corrosion products was of interest. Any soluble salts of the chloride, such as displaced (from oxide/salt mixture) sodium chloride on the surface would not be seen unless incorporated into adherent corrosion products. Chloride was identified in both raster scans and point analysis with EDS.

The chloride was always associated with areas that showed even the smallest amount of attack as shown through the point chemical analyses (Figure 5-13) of the SEM micrograph in Figure 5-12. Figure 5-12 shows the SEM micrograph of an apparent growing pit for TD17 near the TIG closure weld region and Figure 5-13 shows a select number of the EDS spectra. The spots 1, 3, 4, and 6 all were found with chloride (EDS spectra shown for 1 and 6), while spots 2 and 5 did not.

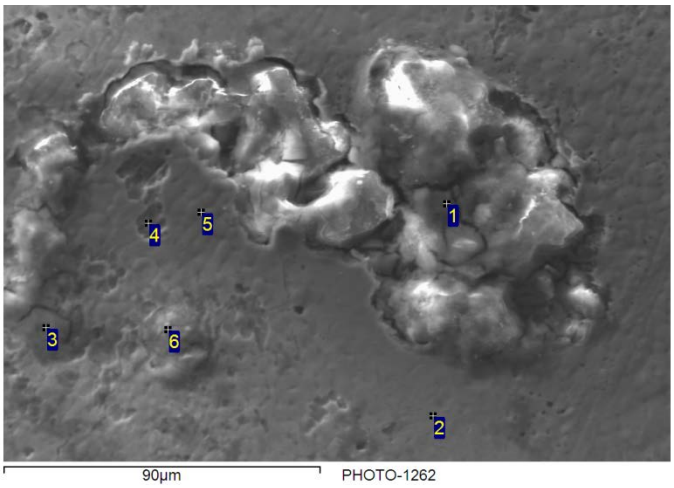

Figure 5-12 SEM micrograph (600x) of a pit in the TIG closure weld region of teardrop coupon TD17 with identified spots where a chemical analysis was performed (See Figure 4-13 for select spectra)

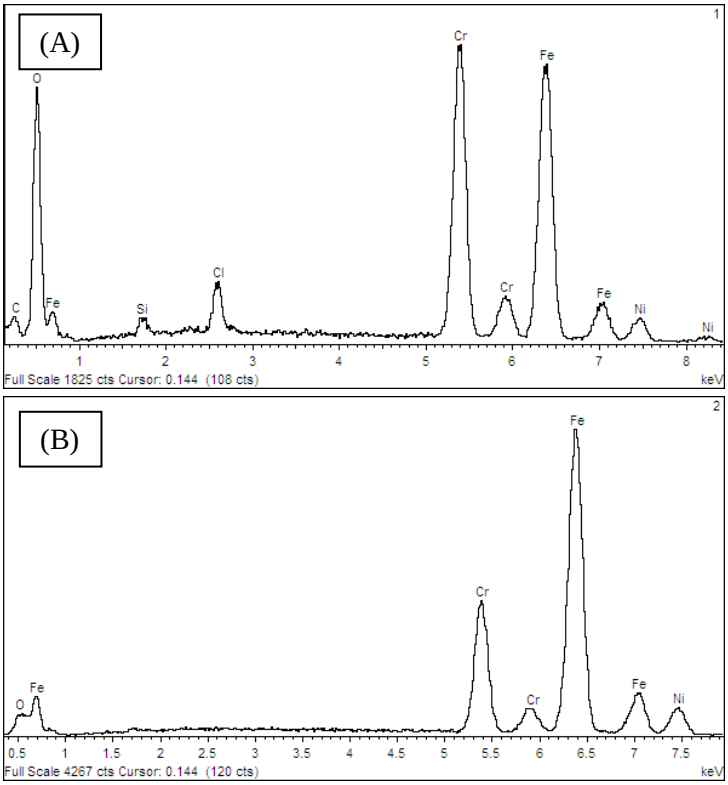

Figure 5-13 EDS spectra for spots identified on the SEM micrograph in Figure 5-12: (A) spot 1; (B) spot 2; (C) spot 5; and (D) spot 6

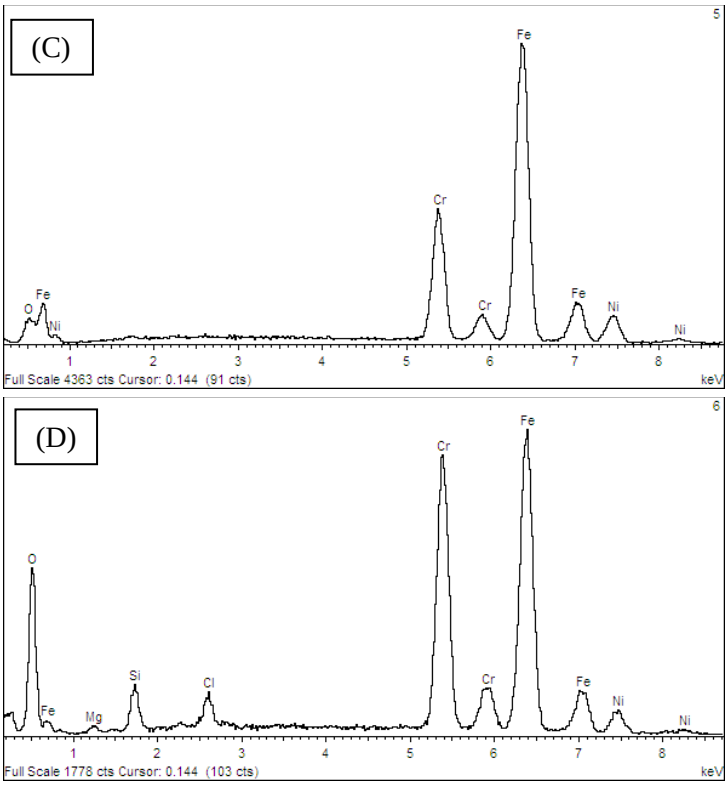

Figure 5-13 EDS spectra for spots identified on the SEM micrograph in Figure 5-12: (A) spot 1; (B) spot 2; (C) spot 5; and (D) spot 6

Plutonium was found in some areas where pitting had occurred but was not associated with all pitting as shown by the data in Figure 5-13. In all cases but one, no cations were identified within the pit. In one pit that was still filled with corrosion products, magnesium was identified.

6.0 Discussion

In this Phase II, Series 2 testing, the lower water loading in the test vessel had a significant effect on the corrosion. Over the two-year period of the test, pitting was the only localized corrosion observed; whereas during the testing associated with Phase I and Phase II, Series 1, SCC was observed within approximately 150 days. The water loading for Phase II, Series 2 was slightly less than 0.2% while for the previous testing was approximately 0.5 to 0.6%. Similarly, the RH inside the Series 2 test containers was lower at 35-40% versus 50-55% for Phase II, Series 1 test vessels. These results are in contrast with the literature which report a greater susceptibility at RH values closer to the salt deliquescence point (approximately 22% in this case for chlorocalcite present in the oxide/salt mixture), but consistent with LANL SCC observations for pure salts and oxide/salt mixtures [5, 6, 12]. The degree of pitting as measured by a qualitative assessment of the area pitted was found to progress with time indicating that corrosion had not ceased. Under these conditions and with sufficient time, SCC cannot be ruled out.

Under these less corrosive conditions of the Phase II, Series 2 test, the exposure condition or location of the exposed surface, i.e. salt or vapor exposed, was found also to affect the observed corrosion. The pitting was greater on surfaces that were exposed to the oxide/salt mixture and is attributed to close proximity of the surface to both moisture and chlorides.

Vapor exposed surfaces, however were found to corrode, but with additional factors that attributed to initiation. The corrosion on vapor-exposed surfaces is more difficult since chlorides need to migrate to these surfaces. Chlorides were found associated with the pitting observed on the TIG closure welds; however, the mechanism cannot be determined from the current data set. The remnant weld oxide made these areas more susceptible as shown by the greater pitting observed on the oxide-covered surfaces. This result reinforces similar literature results [11]. Additionally, the work hardened area in the vapor space, where microstructural differences from the surrounding metal would exist, was more susceptible to pitting. These results are similar to those seen previously and have direct significance to the ICCWR where a remnant weld oxide exists.

The complete application of this data set to the 3013 container environment is limited, however, since the last two test vessels opened, Vessel B and C, showed a fairly large oxygen concentration in the post-test analysis and had varying humidity levels over the test period. Vessel A showed no oxygen present in the post-test gas analysis and had a constant humidity level over the 131 days in test. Both the higher oxygen concentration and the higher humidity level in Vessels B and C could contribute to greater corrosion. The pitting observed in Vessel A, however, was far less than that observed in the previous testing for similar time frames where cracking was observed. A lower water loading in a 3013 container does significantly decrease the corrosion.

Additional analysis of the teardrop coupons from this test series would be beneficial. Specifically, an analysis of pit depth in comparison with those measured from previous test coupons would provide a good quantitative measure for the change in corrosion with water loading. The recent acquisition of a laser confocal microscope would facilitate such measurements. Also, serial metallography on pitted areas of the coupons is recommended since the presence of small subsurface cracks initiating from the pits could be determined. As seen in Phase II, Series 1 test, these small subsurface cracks occurred prior to cracks being observed on the surface at longer times [4].

Important aspects of this work and the other tasks performed under the 2009 corrosion test plan [1] along with the results from the destructive evaluation of 3013 storage containers [13] has shown that the closure weld region of the 3013 inner container is the most vulnerable area for failure and leakage of corrosive vapor species to the outer container, thus possibly limiting the 50-year lifetime of the storage container. In 2014, a new corrosion plan was developed and supersedes the 2009 plan [14]. This new plan has two main components: (1) surveillance activities that determine the extent of corrosion within the ICCWR and that enhance assessment of the inner container for a through-wall failure of the inner container; and (2) small-scale testing to develop the technical basis for estimating future corrosion risk.

7.0 Conclusion

With the completion of Phase II, Series 2 testing, SRNL has completed their contributions to the 2009 corrosion test plan for evaluating the impact of SCC on the 3013 container.

During Phase I testing at high initial moisture levels (0.35 to 1.24 wt%), the room-temperature corrosion of 304L exposed to a series of plutonium oxide/chloride salt mixtures ranged from superficial staining to pitting and stress corrosion cracking (SCC). 304L teardrop coupons that exhibited SCC were directly exposed to a mixture composed of 98 wt % PuO_2, 0.9 wt % NaCl, 0.9 wt % KCl, and 0.2 wt % $CaCl_2$. Cracking was not observed in a 316L teardrop coupon.

Pitting was also observed in this environment for both 304L and 316L with depths ranging from 20 to 100 µm. Neither pitting nor SCC was observed in mixtures with a greater chloride salt concentration (5 and 28 wt %). These results demonstrated that for a corrosive solution to form a balance existed between the water loading and the salt chloride concentration so that conditions for corrosion were not present. This chloride solution results from the interaction of loaded water with the concentration of the hydrating $CaCl_2$ salt.

In Phase II, Series 1 tests, the SCC results were shown to be reproducible with cracking occurring in as little as 85 days. The approximate 0.5 wt% moisture level was found to result in an initial relative humidity of ~55% within the small-scale vessels. Pits were found to be associated with cracks and appeared to act as initiators for the cracking. In a vapor-space only exposure, the weld oxide, which results from the TIG closure weld used to fabricate the teardrop coupon, was also shown to be more susceptible to pitting corrosion than a surface free from weld oxide. This result has important implications for the closure weld of the 3013 inner can since the weld oxide on the can internal surface cannot be removed.

The results from the Phase II, Series 2 tests further demonstrated the significance of forming a solution with a critical chloride concentration for corrosion to proceed. 304L teardrop coupons were found to corrode only by pitting with a similar oxide/salt mixture as used in Phase II, Series 1 testing but with a lower water loading of 0.2 wt%. These tests had a test period twice that for the Series 1 testing. The exposure condition was also found to impact the corrosion with salt-exposed surfaces showing lower corrosion resistance. Additional analyses of the Series 2 coupons are recommended especially for determining the presence of subsurface cracks.

Data generated under the 2009 3013 corrosion test plan, as was presented here, increased the understanding of the corrosion process within a sealed 3013 container. Along with the corrosion data from destructive evaluations of 3013 containers, ICCWR has been identified as the most vulnerable area on the inner can where corrosion may lead to corrosive species leaking to interior surface of the outer container, thereby jeopardizing the integrity. A new corrosion plan has been designed that will characterize the corrosion at the ICCWR of 3013 DEs as well as parameters affecting this corrosion.

8.0 References

1. R. S. Lillard, D. K. Veirs, J. M. Berg, L. A. Worl, J. M. Duffey, K. A. Dunn, R. R. Livingston, P. E. Zapp, and J. W. McClard, "Test Plan for Determining the Susceptibility of 3013 Containers to Stress Corrosion Cracking," LA-UR-09-02953, June 2009

2. "Stabilization, Packaging, And Storage of Plutonium-Bearing Materials", DOE-STD-3013-2004, U. S. Dept. of Energy, 2012

3. P. E. Zapp and J. M. Duffey, "Status Report for the SRNL 3013 Corrosion Tests," SRNS-STI-2008-00093, October 2008

4. J. I. Mickalonis and J. M. Duffey, "SRNL Phase II Shelf Life Studies – Series 1 – Room Temperature and High Relative Humidity," SRNL-STI-2012-00530, Revision 0, September 2012

5. S. Shoji and N. Ohnaka, "Effects of Relative Humidity and Kinds of Chlorides on Atmospheric Stress Corrosion Cracking of Stainless Steels at Room Temperature," Boshoku Gijutsu(Corros. Eng.), 1989

6. T. Shimose, A. Takamura, K. Mori, and K. Shimogori, "Stress Corrosion Cracking of Austenitic Stainless Steels in Chloride Solutions," Trans. JIM, 1965

7. J. I. Mickalonis and J. E. Duffey, "Relative Humidity Tests in Support of the 3013 Storage and Surveillance Program," SRNL-STI-2010-00409, August

8. D. K. Veirs, "Gas generation from water adsorbed onto pure plutonium dioxide powder," Proceedings of the Materials Research Society Symposium 893, Actinides 2005 - Basic Science, Applications and Technology, Paper No. 0893-JJ07-03.1

9. Leak Test Reports, Job Number SRNL-HPL-2010-4354, 2010

10. J. I. Mickalonis, "Assessment of Residual Stresses in SRS and Hanford 3013 Inner and Convenience Cans," SRNL-STI-2009-00121, Revision 0, March 2009

11. A. H. Tuthill and R. E. Avery, "Heat Tint on Stainless Steels Can Cause Corrosion Problems," Materials Performance, Vol (2), 1999

12. Personal communications with K. Veirs and J. Duque, 2014

13. J. I. Mickalonis, "3013 DE Inner Container Closure Weld Corrosion Evaluation," SRNL-STI-2013-00527, Revision 0, September 2013

14. J. M. Berg et al., “Test Plan for Assessing Potential for Stress Corrosion Cracking in the 3013 Inner Container Closure Weld Region (FY2014),” LA-UR-14-20785, June 2014

15. D. G. Kolman, “A Review of the Potential Environmentally Assisted Failure Mechanisms of Austenitic Stainless Steel Storage Containers Housing Stabilized Radioactive Compounds,” Corrosion Science, Vol 43 (1), pp 99-125, 2001

16. J. I. Mickalonis and K. A. Dunn, “ Residual Stresses in 3013 Containers,” JNMM, Vol 38 (2), pp 31-38, 2010